

## Tunable terahertz metamaterials with negative permeability

H. Němec,<sup>1</sup> P. Kužel,<sup>1,\*</sup> F. Kadlec,<sup>1</sup> C. Kadlec,<sup>1</sup> R. Yahiaoui,<sup>2</sup> and P. Mounaix<sup>2</sup>

<sup>1</sup>*Institute of Physics, Academy of Sciences of the Czech Republic, Na Slovance 2, 182 21 Prague 8, Czech Republic*

<sup>2</sup>*Centre de Physique Moléculaire Optique et Hertzienne, Université Bordeaux I, CNRS UMR 5798, 351 Cours de la Libération, 33405 Talence Cedex, France*

(Received 26 March 2009; revised manuscript received 25 May 2009; published 24 June 2009)

We demonstrate experimentally and theoretically dielectric metamaterials exhibiting a tunable range of negative effective permeability in the terahertz spectral region (0.2–0.36 THz). Our structures consist of an array of intrinsically nonmagnetic rods made of an incipient ferroelectric SrTiO<sub>3</sub> which shows a high tunable permittivity. The magnetic response and its tuning are achieved by a temperature control of the permittivity of SrTiO<sub>3</sub>, which defines the resonant confinement of the electromagnetic field within the rods.

DOI: [10.1103/PhysRevB.79.241108](https://doi.org/10.1103/PhysRevB.79.241108)

PACS number(s): 42.25.Bs, 77.84.–s, 78.20.Bh, 78.20.Ci

The concept of metamaterials enables the development of structures exhibiting on-demand optical properties not found in nature. In particular, metamaterials with simultaneously negative dielectric permittivity and magnetic permeability<sup>1</sup> offer possibilities of breaking previously established limits of wave optics.<sup>2</sup> While negative permittivity related to the plasma resonance occurs in most metals in a broad spectral range, negative permeability does not naturally occur beyond the gigahertz frequencies.

Most terahertz and optical metamaterials reported so far were based on miniaturizing the concept of structured composites with patterned metallic subwavelength inclusions<sup>3,4</sup> first introduced at microwave frequencies.<sup>5</sup> Indeed, several metamaterial structures based on subwavelength metallic patterns were prepared using photolithography or electron-beam lithography, and their resonant properties were demonstrated in the THz (Refs. 3 and 6–8) and near infrared ranges.<sup>4,9</sup>

The properties of metamaterials rely on strong electromagnetic resonances, and, consequently, their effective electromagnetic behavior and the aimed applications are restricted to narrow spectral intervals. Active spectral tuning of the metamaterial resonance then appears as highly desirable for broadband applications. This is very difficult to achieve in the metallic-based structures since their properties are controlled mainly by the geometry;<sup>6</sup> numerical simulations revealed that replacing metal by a narrow band semiconductor in a split ring may lead to the tunability of the resonance in the THz range.<sup>10</sup> Recently, control by electric field<sup>6,11</sup> or by optical illumination<sup>7</sup> of a metamaterial resonance strength was achieved and optical switching between two metamaterial resonances at 0.85 and 1.05 THz was experimentally demonstrated.<sup>8</sup> In these works the investigated metamaterials exhibited a purely electric response and the tuning and switching of the resonance was achieved by a dynamical modification of a split-ring capacitance or by its short-circuiting.

In this Rapid Communication we report on a demonstration of a tunable metamaterial exhibiting a negative effective permeability in the terahertz spectral range. Our samples consist of a row of high permittivity rods made of SrTiO<sub>3</sub> (STO) thin single crystal plate [Fig. 1(a)]. STO is known to exhibit a high dielectric tunability in the THz range while its dielectric losses remain at an acceptable level (the loss tan-

gent is about 0.025 at 0.25 THz).<sup>12</sup> First, plane parallel wafers of STO were prepared by mechanical polishing with a thickness of  $t=52\ \mu\text{m}$ ; the thickness of some samples was reduced down to  $t=22\ \mu\text{m}$  by a subsequent wet etching in orthophosphoric acid (H<sub>3</sub>PO<sub>4</sub>). A series of grooves with a width  $d$  and period  $L$  (structure A:  $d=33\ \mu\text{m}$ ,  $L=75\ \mu\text{m}$ , and  $t=52\ \mu\text{m}$ ; and structure B:  $d=28\ \mu\text{m}$ ,  $L=96\ \mu\text{m}$ , and  $t=22\ \mu\text{m}$ ) were drilled in the wafers by femtosecond laser micromachining. The technological challenge was to fabricate a large area pattern in a very thin brittle material. The grooves were directly etched by a Yb:KGW 1.03  $\mu\text{m}$  femtosecond laser at Alphanov technological center.<sup>13</sup> The ultrafast regime offers an enhanced control in producing the desired microstructures as the laser energy absorption occurs on a time scale much faster than the heat transport and the electron-phonon coupling. The resulting patterns covered areas up to  $2.5 \times 3\ \text{mm}^2$ .

The investigated metamaterials are obviously birefringent. While their response is purely electrical for the electric field polarized parallel to the rods ( $p$  polarization), a series of Mie resonances accompanied by an effective magnetic response is expected for the  $s$  polarization ( $E\parallel x$ ).<sup>14</sup> The resonant behavior is closely connected to the high value of the permittivity in STO ( $\sim 300$  at room temperature in the sub-THz range). The wave front of an incident plane electromagnetic wave undergoes a strong distortion close to the metamaterial in order to satisfy simultaneously the continuity and discontinuity conditions of tangential and normal electric-field components at the STO-air interfaces, respectively. The electric field, which develops inside an STO bar, is then predominantly tangential close to the surface of the bar. This leads to the creation of displacive eddy currents within the bar cross section [as shown in Fig. 1(b)], which enhance the magnetic field in STO polarized along the bar. A resonant behavior is then expected at specific frequencies.

The effective properties of the metamaterials can be tuned over a broad spectral range owing to the dielectric tunability of the STO crystal.<sup>15</sup> Similar effects were observed recently in a three-dimensional structure fabricated with millimeter-sized Ba<sub>0.5</sub>Sr<sub>0.5</sub>TiO<sub>3</sub> ceramic cubes designed for the microwave spectral range.<sup>16,17</sup> Resonant behavior and negative refractive index in the microwave range were also reported for a structure consisting of Ba<sub>0.5</sub>Sr<sub>0.5</sub>TiO<sub>3</sub> ceramic rods enclosed between two metallic sheets separated by a subwave-

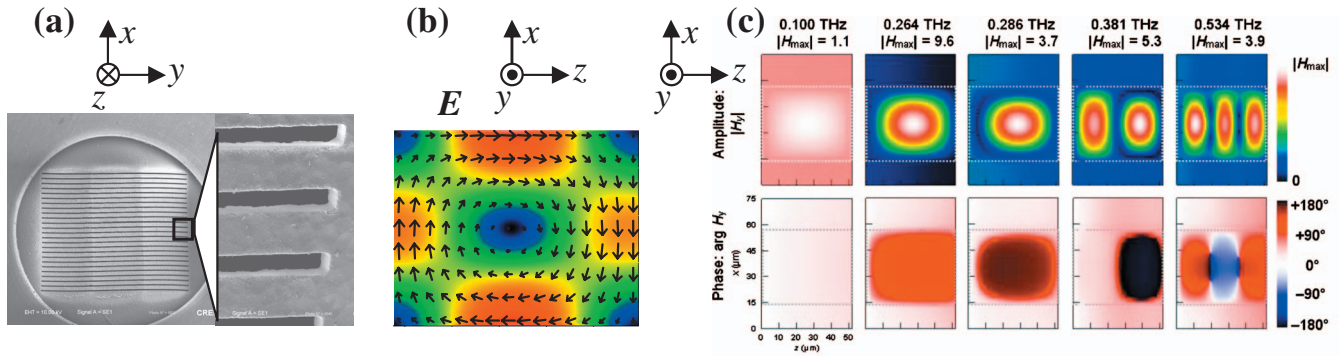


FIG. 1. (Color) (a) Scanning electron microscopy image of an investigated sample (structure B); polarization of the incident wave:  $E_{\parallel}x$  and  $H_{\parallel}y$ . (b) Spatial distribution of the electric field inside an STO rod at 0.264 THz. (c) Spatial distribution of the resonant magnetic field  $H_y$  in a single unit cell of the metamaterial illuminated by a plane monochromatic wave with unitary amplitude. Dotted rectangles indicate the cross section of STO rods. Above the plots the frequencies of the incident waves and the maxima  $|H_{\max}|$  of the amplitude scale for each case are indicated. Top panels: amplitude; bottom panels: phase. Data in (b) and (c) were calculated for structure A at room temperature.

length distance.<sup>18</sup> In contrast to our work, Peng *et al.*<sup>18</sup> employed radiation with electric-field vector polarized parallel to the rods and the resonant behavior was essentially related to a mutual interaction of individual resonators (i.e., to a higher-order dispersion branch) in the two-dimensional photonic crystal.<sup>19</sup>

We studied the electromagnetic behavior of the structures using a multidimensional transfer matrix method.<sup>20</sup> In these calculations the structures were irradiated by a plane monochromatic wave with unitary magnetic field ( $H_{\text{inc}}=1$ ). The transmitted and reflected fields were obtained, and the spectra of effective permittivity  $\epsilon_{\text{eff}}$  and permeability  $\mu_{\text{eff}}$  were retrieved from the transmission and reflection functions.<sup>21</sup>

Experimentally we characterized the metamaterial response using time-domain THz spectroscopy,<sup>22</sup> which employs broadband ultrashort THz pulses for probing. The transmittance spectra of self-standing metamaterials versus temperature shown in Fig. 2 were measured in a usual experimental setup for this technique.<sup>22</sup> Here 250-ps-long time-domain scans were acquired, resulting in 4 GHz frequency resolution. The transmittance amplitude exhibits a pronounced temperature-dependent dip corresponding to the

lowest Mie resonance. At room temperature structures A and B exhibit the dips at 0.265 and 0.360 THz, respectively.

The frequencies of the Mie resonances depend essentially on the optical thickness of the rods in the THz range, i.e., on their permittivity and physical dimensions. Since the permittivity of STO increases considerably upon cooling due to softening of the ferroelectric soft mode ( $\epsilon \approx 1250$  at 100 K),<sup>15</sup> the resonant frequency of the STO-based metamaterial redshifts upon cooling. This is demonstrated in Fig. 2 where the dip in transmittance shifts from 0.29 THz at 324 K down to 0.20 THz at 180 K for structure A and from 0.36 THz at 300 K down to 0.20 THz at 120 K for structure B. Well-established literature values of the temperature dependence of the STO soft mode<sup>15</sup> were used in the simulations. As observed in Fig. 2 the positions of the first Mie resonance obtained experimentally and in the simulations display very good agreement at all temperatures studied and for both structures investigated.

Direct experimental verification of the magnetic nature of the resonance was performed at room temperature. Simultaneous determination of complex permeability and permittivity in the far-infrared region is not a routine task. In prin-

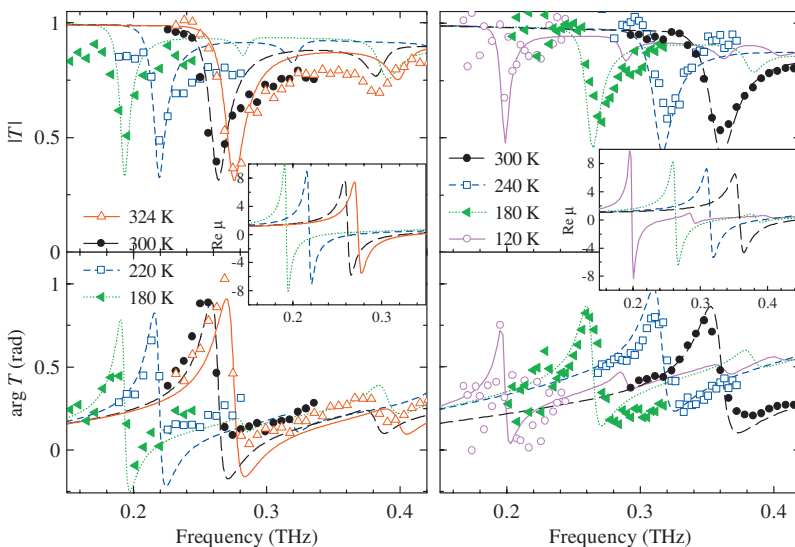


FIG. 2. (Color) Transmittance spectra (amplitude and phase) of the metamaterials for a few representative temperatures (left panel: structure A; right panel: structure B). Points: measurements; lines: calculations using transfer matrix method. Insets: real part of the permeability retrieved from the simulations.

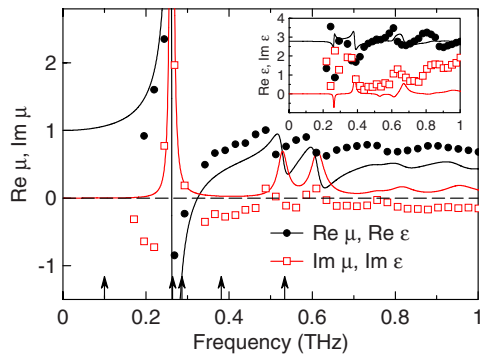


FIG. 3. (Color online) Effective complex magnetic permeability of sample A; symbols: experiment, solid lines: simulations. Arrows indicate frequencies shown in Fig. 1(c).

principle, these quantities can be determined from complex reflectance and transmittance spectra.<sup>21</sup> While the complex transmittance spectrum can be easily measured in the THz range, the determination of the reflectance phase with a high precision, so as to allow a subsequent unambiguous determination of optical properties, is a challenging task requiring specific experimental approaches (see Ref. 23 and references therein). Alternatively, the complex permeability and permittivity can be retrieved from spectra of time-separated pulses corresponding to internal reflections in the sample<sup>24</sup> provided that the sample is sufficiently thick to enable this approach. In order to take advantage of this possibility we put the investigated metamaterial into optical contact with a 2-mm-thick high-resistivity silicon wafer that was polished to achieve an excellent plane parallelism of input and output faces ( $<1 \mu\text{m}$ ). The THz wave transmitted through this structure consists of a series of pulses (separated in time by about 45 ps) originating from internal reflections in the silicon wafer. The time-windowing approach allows us to analyze their spectra one by one<sup>25</sup> and to retrieve the complex permeability and permittivity<sup>21,24</sup> from the complex transmittance and reflectance of the metamaterial encoded in these signals.

At room temperature, the magnetic permeability is experimentally found to be negative between 0.26 and 0.30 THz for structure A and its dispersion agrees well with the Lorentzian shape found in the simulations (Fig. 3). The experimentally observed broadening of this resonance ( $\Delta f_{\text{exp}} \approx 23 \text{ GHz}$ ) is essentially due to the time-windowing procedure used for the retrieval of permittivity and permeability.<sup>26</sup> The intrinsic resonance width found in the simulations is  $\Delta f_{\text{sim}} = 7 \text{ GHz}$ , and it is determined merely by the dielectric losses in STO. The effective permittivity of the metamaterial shows only weak resonances; in particular it varies between 2.4 and 3.2 below 0.35 THz. This value is very low as compared to the permittivity of the STO single crystal, and the difference is related to the fact that STO rods and air gaps act as capacitors in series for the long-wavelength  $s$ -polarized radiation.<sup>27</sup>

An analysis of the spatial distribution of the magnetic field intensity allows a deeper insight into the physics of the problem. The calculated distributions of  $H_y$  inside the unit cell [see Fig. 1(c)] were analyzed within the frame of Pend-

ry's field averaging procedure.<sup>28</sup> Following this procedure, the average magnetic field intensity  $H_{\text{ave}}$  inside the metamaterial is equal to the  $H_y$  value at the corner of the unit cell outside the STO rods<sup>28</sup> while the magnetic induction  $B_{\text{ave}}$  is calculated as an average over the surface delimited by a contour loop of the unit cell. The proportionality constant between these two averaged quantities then provides an estimate of the effective permeability:  $\mu_{\text{eff}} = B_{\text{ave}}/H_{\text{ave}}$ .

In Fig. 1(c) each of the plots represents the unit cell of structure A;  $H_{\text{ave}}$  reaches values comparable to  $\sim 1$  over the whole spectrum studied. At low frequencies well below the Mie resonances (i.e., at  $f \leq 0.1 \text{ THz}$ ) the standard effective medium approximation is valid and the effective magnetic permeability is very close to unity (cf. appropriate frequencies in Fig. 3). A nearly spatially uniform magnetic field in phase with the incident wave corresponds to this case, and its maximum amplitude ( $H_{y,\text{max}} = 1.1$ ) exceeds that of the incident wave at 0.1 THz only by 10%. For the first Mie resonance ( $f = 0.264 \text{ THz}$ ) the field is localized in the rods and the peak enhancement is nearly tenfold; the phase shift of  $\sim 90^\circ$  between the internal and incident magnetic field also illustrates the resonant behavior. The average magnetic induction, which determines the effective magnetic permeability, thus coincides very well with the strong imaginary part of  $\mu_{\text{eff}}$  observed at  $f = 0.264 \text{ THz}$  (Fig. 3). Slightly above the resonant frequency ( $f = 0.286 \text{ THz}$ ) the field amplitude remains high while the phase approaches  $180^\circ$  leading to a negative value of  $\mu_{\text{eff}}$ . The antisymmetric profile of  $H_y$  associated with the second Mie resonance ( $f = 0.381 \text{ THz}$ ) leads to a weak average magnetic induction despite its relatively strong enhancement ( $H_{y,\text{max}} = 5.3$ ). In turn, there is no visible magnetic resonance around  $f = 0.381 \text{ THz}$  in Fig. 3. Similarly, the essentially symmetric character of the field profile at the third resonance (0.53 THz) leads to a pronounced magnetic response in agreement with the measurements.

The simulations show that further lowering of the temperature would shift the resonance down to 0.13 THz at 100 K and that the STO losses remain sufficiently low to retain a negative magnetic permeability. The magnetic permeability

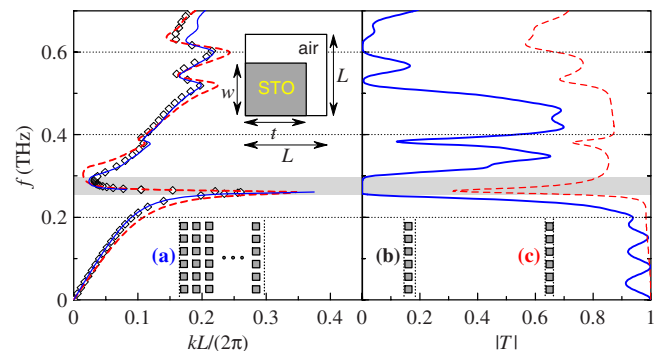


FIG. 4. (Color online) Dispersion curves (left panel) and amplitude transmission functions (right panel) of the investigated STO metamaterials calculated by the transfer matrix method. Inset: unit cell ( $L = 75 \mu\text{m}$ ,  $t = 52 \mu\text{m}$ , and  $w = 42 \mu\text{m}$ ). Investigated structures: (a) sample composed of 16 unit cells along  $z$ -axis (solid line); (b) single unit cell along  $z$ -axis including 23- $\mu\text{m}$ -thick air spacer (symbols); (c) single period along  $z$ -axis without the air spacer corresponding to the evaluations shown in Fig. 3 (dashed line).

retrieved from the simulated transmittance and reflectance spectra exhibits very similar behavior for all investigated temperatures, and in particular it shows a range of negative values (as seen in the inset of Fig. 2). With decreasing temperature a continuous redshift of the interval where the negative permeability occurs is observed. These findings let us infer that a negative effective permeability can be achieved with our structures in the spectral range of 0.13–0.45 THz. It should be emphasized that, in principle, the THz permittivity of STO can be also controlled by a bias electric field.<sup>29</sup> This would open an interesting perspective of electric-field tuning of the magnetic metamaterial response.

The simulations also indicate that the observed resonances are determined by the geometry of the individual rods and not by the coupling between them. In this sense our structure can be considered as a thin-film metamaterial with well-defined effective permeability and permittivity, but it can be in principle extended to a bulk metamaterial by forming, e.g., a square lattice of the rods. This is demonstrated in

Fig. 4: it is obvious that the dispersion curves are semiquantitatively the same for a “bulk” metamaterial composed of 16 layers and a “thin-film” metamaterial composed of a single layer. In addition, both  $\epsilon_{\text{eff}}$  and  $\mu_{\text{eff}}$  are found to exhibit very similar spectra in the bulk and thin-film structures.

In conclusion, we have presented THz metamaterials showing a tunable spectral interval where the magnetic permeability reaches negative values. These values were established both theoretically and experimentally. The demonstrated principle represents a step forward toward a metamaterial with negative refractive index capable of covering continuously a broad range of THz frequencies and opens a path for the active manipulation of millimeter and submillimeter beams.

The financial support of the Ministry of Education of the Czech Republic (Project No. LC-512) and of the Grant Agency of ASCR (Project No. A100100907) is gratefully acknowledged.

\*kuzelp@fzu.cz

<sup>1</sup>R. A. Shelby, D. R. Smith, and S. Schultz, *Science* **292**, 77 (2001).

<sup>2</sup>J. B. Pendry, *Phys. Rev. Lett.* **85**, 3966 (2000).

<sup>3</sup>T. J. Yen, W. J. Padilla, N. Fang, D. C. Vier, D. R. Smith, J. B. Pendry, D. N. Basov, and X. Zhang, *Science* **303**, 1494 (2004).

<sup>4</sup>Stefan Linden, Christian Enkrich, Martin Wegener, Jiangfeng Zhou, Thomas Koschny, and Costas M. Soukoulis, *Science* **306**, 1351 (2004).

<sup>5</sup>D. R. Smith, W. J. Padilla, D. C. Vier, S. C. Nemat-Nasser, and S. Schultz, *Phys. Rev. Lett.* **84**, 4184 (2000).

<sup>6</sup>Hou-Tong Chen, Willie J. Padilla, Joshua M. O. Zide, Arthur C. Gossard, Antoinette J. Taylor, and Richard D. Averitt, *Nature (London)* **444**, 597 (2006).

<sup>7</sup>Hou-Tong Chen, Willie J. Padilla, Joshua M. O. Zide, Seth R. Bank, Arthur C. Gossard, Antoinette J. Taylor, and Richard D. Averitt, *Opt. Lett.* **32**, 1620 (2007).

<sup>8</sup>Hou-Tong Chen, John F. O’Hara, Abul K. Azad, Antoinette J. Taylor, Richard D. Averitt, David B. Shrekenhamer, and Willie J. Padilla, *Nat. Photonics* **2**, 295 (2008).

<sup>9</sup>C. M. Soukoulis, S. Linden, and M. Wegener, *Science* **315**, 47 (2007).

<sup>10</sup>J. Han and A. Lakhtakia, *J. Mod. Opt.* **56**, 554 (2009).

<sup>11</sup>O. Paul *et al.*, *Opt. Express* **17**, 819 (2009).

<sup>12</sup>H. Němec, P. Kuzel, L. Duvillaret, A. Pashkin, M. Dressel, and M. T. Sebastian, *Opt. Lett.* **30**, 549 (2005).

<sup>13</sup><http://www.alphanov.com>

<sup>14</sup>S. O’Brien and J. B. Pendry, *J. Phys.: Condens. Matter* **14**, 4035 (2002).

<sup>15</sup>P. Kužel and F. Kadlec, *C. R. Phys.* **9**, 197 (2008).

<sup>16</sup>Qian Zhao, Lei Kang, B. Du, H. Zhao, Q. Xie, X. Huang, B. Li, J. Zhou, and L. Li, *Phys. Rev. Lett.* **101**, 027402 (2008).

<sup>17</sup>Q. Zhao *et al.*, *Appl. Phys. Lett.* **92**, 051106 (2008).

<sup>18</sup>Liang Peng, Lixin Ran, Hongsheng Chen, Haifei Zhang, Jin Au Kong, and Tomasz M. Grzegorzczak, *Phys. Rev. Lett.* **98**, 157403 (2007).

<sup>19</sup>K. Vynck, D. Felbacq, E. Centeno, A. I. Căbuz, D. Cassagne, and B. Guizal, *Phys. Rev. Lett.* **102**, 133901 (2009).

<sup>20</sup>J. B. Pendry and A. MacKinon, *Phys. Rev. Lett.* **69**, 2772 (1992).

<sup>21</sup>D. R. Smith, S. Schultz, P. Markoš, and C. M. Soukoulis, *Phys. Rev. B* **65**, 195104 (2002).

<sup>22</sup>G. Grüner, *Millimeter and Submillimeter Wave Spectroscopy of Solids* (Springer, Berlin, 1998).

<sup>23</sup>A. Pashkin, M. Kempa, H. Němec, F. Kadlec, and P. Kužel, *Rev. Sci. Instrum.* **74**, 4711 (2003).

<sup>24</sup>H. Němec, F. Kadlec, P. Kužel, L. Duvillaret, and J.-L. Coutaz, *Opt. Commun.* **260**, 175 (2006).

<sup>25</sup>L. Duvillaret, F. Garet, and J.-L. Coutaz, *IEEE J. Sel. Top. Quantum Electron.* **2**, 739 (1996).

<sup>26</sup>A higher resolution could be achieved only by using a substantially thicker silicon wafer. However, as the THz wave undergoes diffraction during the propagation through the Si slab, its diameter after one round-trip may exceed the lateral size of the metamaterial sample and pollute the reflectance signal if a too-thick Si wafer is used. The reflectance amplitude is thus influenced by a systematic error. Our calculations indicate that such an error is probably at the origin of the slightly negative baseline of the magnetic losses ( $\text{Im } \mu$ ) observed in Fig. 3.

<sup>27</sup>C. Kadlec, F. Kadlec, P. Kužel, K. Blary, and P. Mounaix, *Opt. Lett.* **33**, 2275 (2008).

<sup>28</sup>J. B. Pendry, A. J. Holden, D. J. Robbins, and W. J. Stewart, *IEEE Trans. Microwave Theory Tech.* **47**, 2075 (1999).

<sup>29</sup>P. Kužel, F. Kadlec, H. Němec, R. Ott, E. Hollmann, and N. Klein, *Appl. Phys. Lett.* **88**, 102901 (2006).